Cluster formation between an oxadiazole derivative with metal nanoclusters (Ag/Au/Cu), graphene quantum dot sheets, SERS studies and solvent effects

Jamelah S Al-Otaibi (jamelah2019@rediffmail.com)
Princess Nourah bint Abdulrahman University

Y.Sheena Mary
Thushara

Y.Shyma Mary
Thushara

Ravi Trivedi
Bhabha Atomic Research Centre

Brahmananda Chakrabory
Bhabha Atomic Research Centre

Renjith Thomas
St Berchmans College

Research Article

Keywords: SERS, DFT, metal clusters, oxadiazole, solvent effects, ALIE

Posted Date: April 7th, 2022

DOI: https://doi.org/10.21203/rs.3.rs-1517144/v1

Abstract

Interaction of an oxadiazole derivative with Ag/Au/Cu and graphene quantum dots with different solvents is reported theoretically. The adsorption energy is maximum for Cu6 cluster and minimum for Ag6 cluster. The asymmetric charge redistribution between DPMO and M_6s produces an improvement in dipole moment values. The decrease in energy gaps of complexes increased conductivity and metal clusters can be used as a drug sensor. The solvation energies are higher negative in solvent media than in the gaseous media, indicating an enhancement in solvent medium's stability. Wavefunction studies show that there exist significant noncovalent interactions between metal clusters and oxadiazole that facilitates cluster formation. DPMO is found to form stable clusters with graphene which is evident from the enhancement of Raman activity of the system through SERS also enabling it for sensing DPMO in a mixture.

Introduction

One of the most fascinating fields of research is heterocyclic chemistry. Due to their intriguing biological actions, thiazoles, thiadiazoles, indoles and oxadiazoles are among the most important heterocyclic compounds [1]. New infectious diseases have evolved in recent decades, while formerly treated diseases have resurfaced [2]. Despite the urgent need for novel antimicrobial medicines, progress on these agents in slowing [3]. Oxadiazoles have many properties, likeantiviral, antibacterial, anti-neoplastic, antioxidant, antifungal, inhibitors of tyrosinase and cathepsin K [4–10]. Oxadiazole can also significantly contribute to boosting pharmacological activity [11]. Zibotntan, an important anticancer drug and nesapidil as an antihypertensive agent, are one of the commercially available medicines having the oxadiazole molecule [12, 13]. Oxadiazole derivatives are used in a variety of industries, including fluorescent materials, electro-optical devices and high performance materials in the polymer industry [14–17]. Xu et al. reported biological evaluation oxadiazole acetamide moiety as a novel linker [18]. Chortani et al. reported theoretical studies of oxadiazole linked with benzoypyrimidinones [19]. Synthesis and computational studies of three oxadiazoles are reported by Hamdani et al. [20]. Researchers have studied different oxadiazole derivatives as corrosion inhibitors [21]. Some methoxyphenyl compounds are photo sensitizers that are frequently employed in biochemistry, medical therapies, cell and sensor research [22–24]. Oxadiazole was widely employed as a preferred scaffold in drug development [25–27]. It was frequently utilized as bioisoesters for carbonyl containing compound drugs interacting with receptors via hydrogen bonding interactions [28, 29].

Because M_6 is the smallest experimentally created cluster, clusters of six atom of particular have relevance among numerous homo and bimetallic clusters [30, 31]. Several metals shows SERS enhancement [32–40]. SERS of pyridine was reported by Zuo and Jagodzinski utilizing various metals [41]. SERS with gold is used as a sensor for drug monitoring in blood [42]. Mary et al. reported a number of studies of oxadiazole and methoxyphenyl derivatives [43–52].

Cu, Ag and Au, the coinage metals of group XI has rich coordination chemistry as potent reagents [53, 54]. Unlike their silver analogues, derivatives of copper and gold are known as most active complexes in catalysis, allowing for the use of organo-metallic entities in catalysis and materials research [55]. Silver derivatives on the other hand, are the most widely used metal based drugs in a variety of biological applications [56]. Kleinhans et al. reported photo physical effects of T-shaped coinage metal complexes [57]. Coinage metals with a lower oxidation state have been the subject of research into their usage in OLEDs [58]. In the field of coordination chemistry, complexes containing nitrogen donor atoms and coinage metals are commonly encountered protagonists. These compounds are intriguing not only because of their many structural motifs, but also because many investigations on the potential application of these materials have already been completed, demonstrating their versatility [59–61] .A large variety of luminous coinage metal complexes have been reported in the literature [62]. Interaction of 5-(3,4-dimethoxyphenyl)-3-(3-methoxyphenyl)-1,2,4-oxadiazole (DPMO) with M_6 (M = Ag/ Au/ Cu) clusters are predicted in the present work.

Methods

The DFT analysis was used to investigate the essence of proposed structures' structural, chemical, electronic, thermodynamic properties in order to find a viable DPMO drug detector. All M_6 clusters and DPMO were optimized before adsorption process using Gaussian 16 program's B3LYP functional and SDD basis set [63, 64]. Energy and frequency calculations were used to establish the structural integrity and natural existence of adsorbents. To create energetically appropriate and persistent conjugated nano structures, we examined the adsorption process of DPMO on nano metal clusters. We investigated thermodynamic terms, changes in enthalpy, entropy and Gibbs free energy to find thermal stability of DPMO and DPMO-M_6 systems. We conducted a thorough examination of the energy of the HOMO, LUMO, DOS and NBO to get electronic confirmation of the interaction between M6 and DPMO. All DPMO-M_6 systems were optimized in various solvents and key features such as solubility, adsorption properties, and electronic properties were estimated to better understand the biological influence [65, 66]. Reaction sites of DPMO-M_6s were examined using Multi-wavefunction by analyzing ALIE, electron localized function, and noncovalent interactions [67].

Results And Discussion

Optimized geometries of M_6s and DPMO

Fig.1 shows the DPMO and M_6s' structures, FMOS and MEP plot. The electronic properties of DPMO including as HOMO, LUMO and dipole moment were investigated (Table 1). The dipole moment (DM) of DPMO is 4.8758 Debye, indicating that asymmetric charge distribution which is supported by MEP (Fig.1) with reactive sites around primarily on O, N and C atoms. The Fermi level is given as -4.0764 eV, while E_H and E_L values are -6.1875 and -1.9652 eV (table 1). In order to discover a good adsorbent for DPMO, we conducted a comparison analysis and selected three nanoclusters: M_6 (M=Ag/Au/Cu). The bond lengths for Ag/Au/Cu clusters 2.7299, 2.6989 and 2.3781Å respectively which are perfectly consistent with various theoretical conclusions [68]. The M_6s have zero dipole moments, which mean the charges are evenly distributed across the structure. The FMOs energy values were -5.6128/-6.7837/-5.7301 eV and -2.5823/-3.3766/-2.4718 eV respectively for Ag/Au/Cu clusters and the band gaps are, 3.0305/3.4071/3.2683 (table 1) [69].

Table 1 Chemical descriptors (in eV), solvation free energy and dipole moments of DPMO, M_6 clusters and DPMO-M_6 clusters in different solvents

Systems	E_H	E_L	E_g	Hardness	Fermi level	Electrophilicity index	Adsorption energy/SFE (kJ/mol)	Dipole moment (Debye)
DPMO	-6.1875	-1.9652	4.2223	2.1112	-4.0764	3.9354	-	4.8758
Ag_6	-5.6128	-2.5823	3.0305	1.5153	-4.0976	5.5403	-	0
Au_6	-6.7837	-3.3766	3.4071	1.7036	-5.0802	7.5745	-	0
Cu_6	-5.7301	-2.4618	3.2683	1.6342	-4.0960	5.1330	-	0
DPMO-Ag_6	-4.8596	-2.6574	2.2022	1.1011	-3.7585	6.4146	-42.75	11.5349
DPMO-Ag_6 (Toluene)	-4.6864	-2.5576	2.1288	1.0644	-3.6220	6.1626	-65.21	11.8295
DPMO-Ag_6 (Dichloromethane)	-4.6534	-2.6591	1.9943	0.9972	-3.6563	6.7028	-84.79	12.0078
DPMO-Ag_6 (Methanol)	-4.6623	-2.5532	2.1091	1.0546	-3.6078	6.1710	-91.77	12.0472
DPMO-Ag_6 (water)	-4.6661	-2.5551	2.1110	1.0555	-3.6106	6.1755	-93.47	12.0549
DPMO-Au_6	-5.7271	-2.8923	2.8348	1.4174	-4.3097	6.5520	-60.26	12.7971
DPMO-Au_6 (Toluene)	-5.6953	-2.8016	2.8937	1.4469	-4.2485	6.2372	-81.87	13.4181
DPMO-Au_6 (Dichloromethane)	-5.7418	-2.7889	2.9529	1.4765	-4.2654	6.1609	-101.25	13.8383
DPMO-Au_6 (Methanol)	-5.7712	-2.7927	2.9785	1.4893	-4.2820	6.1556	-108.26	13.9609
DPMO-Au_6 (water)	-5.7793	-2.7940	2.9853	1.4927	-4.2867	6.1551	-109.97	13.9888
DPMO-Cu_6	-4.7064	-2.7328	1.9736	0.9868	-3.7196	7.0102	-67.95	11.4988
DPMO-Cu_6 (Toluene)	-4.8180	-2.6950	2.1230	1.0615	-3.7565	6.6469	-88.38	12.3600
DPMO-Cu_6 (Dichloromethane)	-4.9380	-2.6969	2.2411	1.1206	-3.8175	6.5023	-106.64	12.9964
DPMO-Cu_6 (Methanol)	-4.9848	-2.7007	2.2841	1.1421	-3.8428	6.4647	-113.24	13.2090
DPMO-Cu_6 (water)	-4.9965	-2.7018	2.2947	1.1474	-3.8492	6.4563	-114.85	13.2605

Adsorption and desorption processes

To begin, we used the DFT level of theory to examine the structural properties, adsorption energy, thermodynamic properties and other features of DPMO with M_6s in order to find the most energetically favorable conjugated configuration. The DPMO interacts with our studied adsorbents via the oxadiazole ring's O and N atoms. To further understand the adsorption process, we used the following equation to compute the adsorption energies (Eads) of all conjugated configurations, which are reported in table 1 [70]: $E_{ads}= E_{M6\text{-}DPMO} – E_{M6}\text{-}E_{DPMO}$; $E_{M6\text{-}DPMO}$ refers to energy of the conjugated structure; E_{M6} and E_{DPMO} are the energies of M_6 and DPMO, respectively. The thermodynamic properties of conjugated structures were also examined to ensure their thermal stability. Reaction is endothermic if $\Delta H>0$ or exothermic

when ΔH<0 and ΔG tells us whether the DPMO and MCs have a spontaneous interaction (ΔG<0) or not (ΔG>0). The ΔG and ΔH are given as [71, 72]: $\Delta U = U_{M6\text{-}DPMO} - U_{M6} - U_{DPMO}$, where U us the Gibbs free energy (G) and enthalpy (H).

In the adsorption of DPMO-M6 structures, DPMO interacts with M_6s, at distances of 2.2824, 3.1579 (Ag-N/O), 2.1841, 3.0940 (Au-N/O) and 1.9634, 2.9054 (Cu-N/O). The adsorption energies are, highest for Cu6 cluster (-67.95 kJ/mol), lowest for Ag6 cluster (-42.75 kJ/mol) and -60.26 kJ/mol for Au6 cluster. Furthermore, considerable changes in thermodynamic characteristics were observed for different M_6s (table S1). The exothermic, spontaneous and thermodynamically ordered interactions are indicated by the negative values of above. The frequencies of all systems are positive revealing the natural occurrence of the three examined DPMO-M_6 clusters.

Dipole moment and MEP maps

The non-uniform charge distribution over DPMO causes a dipole moment in the molecule. All adsorbents, M_6s, have zero dipole moment due to symmetric charge distribution across entire structure. All conjugated configurations achieved a dipole moment after contact of the DPMO molecule with all M_6s (table 1). The redistribution of charges between DPMO and M_6s causes this improvement in DM. In the case the DM values are 11.5349/12.7971/11.4988 for DPMO-Ag/Au/Cu systems. We found a trend in the amplification of DM due to interaction of M_6s with DPMO as Au > Ag > Cu from the data analysis. This suggests that the DPMO- M_6s charge flow in the case of Au is substantially larger than in the case of other adsorbents, which explains why DPMO and Au_6 have a stronger affinity. By displaying the greater (positively charged) and lower (negatively charged) electrostatic potential areas of a molecule, the MEP map exposes the asymmetric charge distribution. The MEP surface's red to blue color scheme denotes the electron-rich electrophilic attack zone and the electron-deficient nucleophilic attack region, respectively. The MEP maps of DPMO-M_6 structures (Fig.2) indicate reduced change in charge density of the M_6s and DPMO surfaces, indicating that the DPMO and the investigated adsorbents (Ag/Au/Cu) have had unfavorable interactions. Furthermore, the red and blue colors are dispersed across DPMO-M_6. For DPMO- M_6s, on the other hand, red color (reduced electrostatic potential) occupies nearly DPMO. The DPMO section is red, whereas the metal cluster portion is blue, indicating that charge transformation has occurred from the M_6s to the DPMO.

FMOs

The FMOs, HOMO and LUMO, are utilized to explain the idea of adsorbent-adsorbate interaction. Furthermore, because of the availability of electrons than can be donated, HOMO is linked to ionization potential, whereas LUMO energy is linked to the electron affinity due to the lack of electrons. The energy gap (E_g), which is used to characterize the electrical and optical properties of conjugated systems are another important parameter. For DPMO- M_6s (table 1), HOMO energies changed from -5.6128 (Ag_6) to -4.8596 (DPMO-Ag_6), -6.7837 (Au_6) to -5.7271 (DPMO-Au_6), -5.7301 (Cu_6) to -4.7064 (DPMO-Cu_6) and LUMO changed from -2.5823, -3.3766, -2.4718 (Ag/Au/Cu-6) to -2.6574, -2.8923, -2.7328 (DPMO-Ag6/Au6/Cu6). The HOMO is centered on the adsorbent MC in all of the investigated DPMO-M_6s conjugated complexes, while the LUMO is spread largely over DPMO and M_6s (Fig.2). As a result, between M_6s and DPMO, there is a shift in the HOMO and LUMO levels. For DPMO- M_6s changes in E_g have been found, which is validated by PDOS studies. The decreases in E_g have been perceived as 27.33, 16.80 and 39.61% for DPMO-Ag6, DPMO-Au6 and DPMO-Cu6 structures. The decrease in E_g is linked to the nanostructures increased conductivity [73]. As a result, the decrease in E_g for the interaction of DPMO with can cause electrical noise, indicating that M_6s could be used as a DPMO drug sensor.

We also calculated the PDOS to demonstrate the availability of newly created states in energy band and therefore realize the orbital hybridization. In the energy gap of M_6s following interaction with DPMO, as shown in Fig.S1 many energy state may be seen. This suggests that all of the suggested DPMO-M_6s conjugated nanostructures have experiences

orbital hybridization. As a result, the energy gap of all the DPMO- M_6s has reduced, supporting the change in E_g. The E_g and conductivity (σ) is given by $\sigma = AT^{3/2} \exp(-Eg/2kT)$ [74]. Accordingly when energy gap shrinks, the conductivity increases exponentially. This means that the reduction in energy band, which is a critical property for sensing drugs M_6s, generates an electrical signal. Hence the sensitivity of M_6s toward DPMO follows the trend: σ(Cu6) > σ(Ag6) > σ(Au6). As a result, Cu_6 might be said to more sensitive to DPMO than the other two adsorbents and a suitable nanomaterial for detecting DPMO.

Quantum molecular descriptors (QMD)

To decode the details on chemical stability and reactivity of DPMO and M_6s, QMD analyses are required. The QM descriptors are: hardness, $\eta = (E_L-E_H)/2$ and electrophilicity index $\omega = \mu^2/2\eta$ [75]. From table 1, we can observe that η of M_6s has been reduced after interaction with DPMO from 1.5153/1.7036/1.6342 (Ag/Au/Cu) to 1.1011/1.4174/0.9868 (DPMO-Ag/Au/Cu). This indicates that chemical reactivity of the M_6s has increases as compared to bare M_6s. DPMO-MC's softness on the other hand, have increased from their original structures. In summary, DPMO-Cu_6 conjugated structures have been found to have greater variances in hardness and softness, as well as in the electrophilicity index, when compared to Ag_6 and Au_6. As a result, we can deduce that Cu_6 interacts with the MPDO molecule more than other adsorbents.

NBO analysis

Through charge transfer interaction between adsorbate and adsorbents, NBO analysis provides information on bonding and hybridization [76]. It has been estimated the interaction energy between filled and empty NBOs (table S2). We can see that more electronic charge has passed between intra molecular NBOs, suggesting stabilization. The interacting orbitals belonging to oxadiazole ring and neighboring units give maximum energies with highest values for Cu6-DPMO. The Mulliken charges of O1, N5 and N6 of DPMO are -0.257964, -0.146621 and -0.045512 and the corresponding charges in Ag/Au/Cu-DPMO are: -0.233902, -0.112060, -0.164591/-0.215203, -0.102209, -0.238470/-0.223696, -0.122827, -0.240453 (table S3). Due to the interaction of metal cluster and DPMO the charges in oxadiazole ring show large variations. Most of the other charges of DPMO in DPMO-M_6s also show variations due to interaction with metal atoms.

Solvent effects

We optimized the DPMO-M_6s using PCM model and computed SFE, DM, FMOs and E_g among other things, to understand the influence of polar media with different dielectric constants: 2.38 (toluene), 8.93 (dichloromethane), 32.70 (methanol) and 80.40 (water) (table 1) [77]. The SFE of the DPMO-M_6s in solvents follow the same trend as the adsorption energies of DPMO-M_6s with gaseous state with high values for Cu_6-DPMO. This indicates that DPMO-M6 conjugated structures produced slightly higher negative SFE in solvent media than in the gaseous media, indicating an enhancement in solvent medium's stability (table 1). Furthermore, the DM of DPMO-M_6s in solvents has increased as compared to gaseous media, implying that the reactivity and solubility of the examined DPMO-M_6s has increased. The ΔEg of DPMO-M_6s conjugated structures in solvents was also calculated and discussed in order to nominate an electrical sensor for the DPMO. In Au/Cu-DPMO clusters energy gap increases in all solvents while for Ag6-DPMO there is a decrease in the Eg values. It means Au_6 and Cu_6 clusters are good sensors as supported by its solvation or adsorption energies. This is also evident from the Raman spectra (Fig.S2) in which in the finger print regions maximum enhancements are for Au/Cu-DPMO clusters due to SERS effects [78, 79].

Average localized ionization energy (ALIE) assay

The ALIE explains the structure and stability of molecules by the nature of electrons. Oxadiazole formed complex with Ag, Au, and Cu metal sheets. The metal sheets like Ag, Au, and Cu have color from blue to red of scale value from 0.00 to 2.00, and complex size ranges from 9.27 to -7.42, from 7.36 to -7.36 from 8.83 to -6.85 $Å^3$, respectively. Fig.3 shows the ALIE of all three metal complexes. The color blue (range 0.00-0.20Å) represents lone-pairs/unreacted electrons within complexes, and sites are all nitrogen (N), oxygen (O), and metals (Ag, Au, and Cu); like red (range 1.80-2.00Å) represents localized/core electrons of complexes, and sites are all heavy atoms like carbon (C), nitrogen (N), oxygen (O), and metals (Ag, Au, and Cu); in the same way bluish-green (range 0.80-1.10 Å) represents the delocalized/mobile electrons, these produce number of resonance structure of those complexes can explain stability, and also create electron rich and poor sites for potentially chemical reactivity like methoxyphenyl-, 1,2-dimethoxyphenyl-, imidazole- group, and few metals close to molecule [80,81].

Electron localized function (ELF) assay

The ELF explains the structure and stability of molecules by the position of electrons. Oxadiazole-metal cluster showed colors from blue to red mention that probability of electron sites 0.00 to 1.00, and complex size ranges from 9.27 to -7.42, from 7.36 to -7.36, and from 8.83 to -6.85 $Å^{3,}$ respectively. Fig.4 shows the ELF of all three metal complexes. The colored (range 0.80-1.00) noticed that most probability of electrons staying at hydrogen (H) atoms, bonds of C-C, C-N, C-O, and some metals; blue (range 0.00-0.25) noticed that least probability of electrons sites, and also called delocalized/resonance electrons at methoxyphenyl-, 1,2-dimethoxyphenyl-, imidazole- groups with a few metals close to the molecule [82, 83].

Noncovalent interactions (NCI) assay

The NCI explains the stability of complexes by types of hydrogen bonds; these are noncovalent/nonbonded bonds. It is found that there exists significant interaction between the oxadiazole and the clusters. The metal sheets like Ag, Au, and Cu having the color from blue to red scale from -0.05 to 0.05 a.u., are the strength of hydrogen bonds from strong to weak type. Fig.5 shows the NCI of complexes. The formation of strong hydrogen bond from metals Ag, Au, and Cu to hydrogen's in methoxyphenyl-, 1,2-dimethoxyphenyl-, imidazole- groups, and descending order of them is Cu > Ag > Au; like, weak hydrogen/van der Waals hydrogen bonds formation from metals Ag, Au, and Cu to hydrogen's in methoxyphenyl-, from O and N atoms to methoxyphenyl-, 1,2-dimethoxyphenyl- groups and from O in methoxy to hydrogen's in methoxyphenyl-, 1,2-dimethoxyphenyl- groups, and descending order of them is Cu > Au > Ag; alike, the red color notice that hydrogen-hydrogen repulsions, bulky groups repulsions, and aromatic rings repulsions, these interactions between oxadiazole- and methoxyphenyl-, oxadiazole- and 1,2-dimethoxyphenyl-, oxygen and carbon in 1,2-dimethoxyphenyl-, oxygen in methoxy and phenyl- and all metals, and descending order of them is Au > Cu > Ag [84,85].

Prediction of bio-activity through TD-DFT calculations

TD-DFT is always essential for effective molecular modeling. Electronic transition between molecular orbital is a time dependent phenomena [86]. UV absorption spectra and oscillator strength (f) of drug molecule attached with small Ag, Au, and Cu clusters were calculated with TD-DFT method at B3LYP/SDD level of theory to obtain electronic transition states. Our calculated data's for Ag cluster attached drug molecule shows there are six electronic transitions in the UV region as shown in electronic supplementary Fig.S3 with blue vertical lines and the one with highest oscillator strength "0.029" at 7000cm^{-1} which corresponds to the movement of electron from H to L state (where H present HOMO and L present LUMO). This may be attributed to MLCT (metal to ligand charge transfer) .i.e. the charge is transferring from Ag cluster to drug molecule [87] and it is also support our charge transfer mechanism. The other transition are corresponds to H-1 to L, H-2 to L, H-1 to L, H-1 to L, and H to L. Similarly for Au cluster attached with drug molecule exhibit only one electronic transition state with oscillator strength 0.0032 at 15000 cm^{-1} (Fig.S3). In this transition the main contribution comes when electron move from HOMO to LUMO state and it is also ascribed as ligand to metal charge transfer. Similar,

Cu clusters with drug molecule exhibit six electronic transitions in the UV region with highest oscillator strength 0.068 at 7500 cm^{-1} which again due to the jump of electron from the HOMO to LUMO site. The importance of the result obtains from Ag; Cu cluster with drug decides the use of this system in bacterial culturing. Optical density measurements use a wavelength of 600-620 nm to estimate the cell concentration and to track growth pattern [88].

Interaction of Drug and metal cluster + drug over graphene QD sheet

We know graphene is a single-atom thick, two-dimensional sheet of hexagonally arranged carbon atoms. Graphene has free surface π electrons and are capable of forming π–π interactions for loading drug as well as covalent modifications [89, 90]. On the other hand, it is well known that biological activity describes the beneficial or adverse effects of a drug on living matter [91]. If anyhow the biological activity of drug molecule can be increased it will be beneficial for us. To enhance this biological activity, we studied the vibrational Raman properties of present drug molecule over the graphene quantum dots (G-QD). Here we used graphene as a substrate rather than metal surface. The interaction of π electrons (2p orbital) of carbon on graphene with the 2p orbital of oxygen or nitrogen as well as Ag, Au, and Cu increases the signal strength of Raman frequency.

As we can see the Fig.S4, the intensity of Raman activity for drug molecule over graphene QD is 2390au at the frequency 1652.88 cm^{-1} while the individual drug molecule has the intensity1889au at the frequency 1659.05 cm^{-1}. We have also analyzed the Raman activity with metal clusters and found there is a very little bit difference at the frequency level. It can be seen that the Raman activity intensity for Ag_6, Au_6, and Cu_6 attached with drug molecule over graphene QD are 2420au, 2391au, 2253au at the frequency level 1652.88 $cm^{-}1$, 1652.5 cm^{-1}, and 1653.18 cm^{-1} respectively. The Raman vibrational data's for Ag, Au, and Cu clusters with drug molecule over graphene quantum dots shows enhancement of Raman signals. It is very interesting that this combination can be used as a detection of this drug molecule in a biological sample.

Conclusion

The cluster formation of DPMO with different metals was reported with the help of chemical descriptors, solvation effects and wavefunction analysis. Changes in thermodynamic characteristics observed for different M_6s are exothermic, spontaneous and thermodynamically ordered interactions. DPMO-Cu_6 have been found to have greater variances in chemical descriptors when compared to Ag_6 and Au_6 and hence Cu_6 interacts with the MPDO molecule more than other adsorbents. The increase energy gap in Au/Cu-DPMO clusters in all solvents with respect the gaseous state means Au and Cu clusters are good sensors. The cluster formation is stabilized by various noncovalent interactions and it led to favorable change sin electron delocalization in the system .Drug is found to interact with graphene quantum dots also. The enhancement of Raman activity using both clusters indicate it suitability for the development of sensors based on the clusters.

Declarations

Acknowledgments

The authors express their gratitude to Princess Nourah bint Abdulrahman University Researchers Supporting Project number (PNURSP2022R13), Princess Nourah bint Abdulrahman University, Riyadh, Saudi Arabia

Author contribution

Jamelah S.Al-Otaibi: Software, Supervision, manuscript preparation and data analysis

Y.Sheena Mary: Supervision, manuscript preparation, conceiving the problem and data analysis

Y.Shyma Mary: Manuscript preparation, conceiving the problem and data analysis and correction

Ravi Trivedi: Software, Supervision, manuscript preparation and data analysis

Brahmananda Chakrabory: Software, Supervision, manuscript preparation and data analysis

Renjith Thomas: Software, Supervision, manuscript preparation and data analysis

Data availability: The supplementary information files include additional materials

Code availability: No new codes have been created. Existing codes were utilized and quoted correctly

Conflict of interest The authors declare no competing interests

References

1. Jain AK, Vaidya SSharmaA, Ravichandran V (2013) 1,3,4-thiadiazole and its derivatives: a review on recent progress in biological activities. Chem Biol Drug Des 81:557–576. https://doi.org/10.1111/cbdd.12125
2. Reuman M, Daum SJ, Singh B, Wentland MP, Perni RB, Pennock P, Carabateas PM, Gruett MD, .Saindane MT, Dorff PH, .Coughlin SA, .Sedlock DM, .Rake JB (1995) .Lesher, Synthesis and antibacterial activity of some novel 1-substituted 1,4-dihydro-4-oxo-7-pyridinyl-3-quinolinecarboxylic acids, potentiantistaphylococcal agents. J Med Chem 38:2531–2540. https://doi.org/10.1021/jm00014a005
3. Khanum SA, Shashikanth S, Umesha S (2005) Synthesis and antimicrobial study of novel heterocyclic compounds from hydroxylbenzophenones. Eur J Med Chem 40:1156–1162. https://doi.org/10.1016/j.ejmech.2005.04.005
4. Zarudnitskii EV, Pervak II, Merkulov AS, .Yurchenko AA, Tolmachev AA (2008) Trimethylsilyl-1,3,4-oxadiazoles-new useful synthons from the synthesis of various 2,5-disubstituted-1,3,4-oxadiazoles. Tetrahedron 64:10431–10442. https://doi.org/10.1016/j.tet.2008.08.040
5. Tan TM, Chen Y, Kong KH, Bai J, Li Y, Lim SG, Ang TG, Lam Y (2006) Synthesis and the biological evaluation of 2-beneznesulfonylaklyl-5-substituted-sulfanyl-[1,3,4]-oxadiazoles as potential antihepatitis B virus agents. Antivir Res 71:7–14. https://doi.org/10.1016/j.antiviral.2006.02.007
6. V.Girish NF (2014) Synthesis and evaluation of in vitro antimicrobial activity of novel 2-[2-(aroyl)aroyloxy]methyl-1,3,4-oxadiazoles, Russ. J Bioorg Chem 40:330–335. https://doi.org/10.1134/S1068162014030066
7. Aboria AS, Abdel-Rahman HM, Mahfouz NM, El-Gendy MA (2006) A novel 5-(2-hydroxyphenyl)-3-substituted-2,3-dihydro-1,3,4-oxadiazole-2-thione derivatives: promising anticancer agents, Bioorg. Med. Chem. Lett. 14 1236–1246. https://doi.org/10.1016/j.bmc.2005.09.053
8. Ranganatha VL, Khanum SA (2014) Synthesis and evaluation of in vitro antioxidant properties of novel 2,5-disubstituted 1,3,4-oxadiazoles, Russ. J Bioorg Chem 40:206–213. https://doi.org/10.1134/S1068162014020083
9. Khan MTH, Choudhary MI, Khan KM (2005) Atta-ur-Rahman, Structure activity relationships of tyrosinase inhibitory combinatorial library of 2,5-disubstituted-1,3,4-oxadiazole analogues, Bioorg. Med Chem 13:3385–3395. https://doi.org/10.1016/j.bmc.2005.03.012
10. Palmer JT, .Hirschbein BL, Cheung H, Janc JMcCarterJW, Yu WZ (2006) Keto-1,3,4-oxadiazoles as cathepsin K inhibitors. Bioorg Med Chem Lett 16:2909–2914. https://doi.org/10.1016/j.bmcl.2006.03.001
11. Gurupadaswamy HD, Thirusangu P, Avin BRV, Vigneshwaran V, Kumar MVPrashanth, .Abhishek TS, Ranganatha VL, Khanum SA (2014) .Prabhakar, DAO-9(2,5-di(3-aryloxylaryloxymehtyl)-1,3,4-oxadiazole) exhibits p53 induced

apoptogenesis through caspase-3 mediated endonuclease activity in murine carcinoma. Biomed Pharmacother 68:791–797. https://doi.org/10.1016/j.biopha.2014.07.004

12. Khan BA, Zafar S, Mughal EU, Ahmed MN, .Hamdani SS, Akhter T, Haq I, Sadiq A (2018) .Khan, Design and synthesis of novel 1,3,4-oxadiazole derivatives bearing azo moiety as biologically significant scaffolds. Lett Drug Des Discov 15:1346–1355. https://doi.org/10.2174/1507180815666180326152204
13. Ahmaed MN, Sadiq B, Al-Masoudi NA, Yasin KA, Hameed S, Mahmood T, Ayub K (2018) Tahir, Synthesis, crystal structures, computational studies and antimicrobial activity of new designed bis((5-aryl-1,3,4-oxadiazol-2-yl)thio)alkanes. J Mol Struct 1155:403–413. https://doi.org/10.1016/j.molstruc.2017.11.011
14. Petti PMormileL, Laurienzo MP, Malinconico M, Roviello A, Lipson S (2003) Optical properties of a novel alkoxy-substituted poly (p-phenylene 1,3,4-oxadiazoles) for electro-optical devices. Mater Chem Phys 77:945–951. https://doi.org/10.1016/S0254-0584(02)00187-6
15. Casu MB, Imperia P, Schulz B (2002) Electronic structure at the interface between metals and new materials for organic light emitting diodes. Surf Sci 507–510. 666–671. https://doi.org/10.1016/S0039-6028(02)01333-X
16. Lai CK, Ke Y-C, Chien-Shen J-CS, Li W-R (2002) Heterocyclic 1,3,4-oxadiazole as columnar core. Liq Cryst 29:915–920. https://doi.org/10.1080/02678290210129957
17. Patel KD, Prajapati SM, Panchal SN, Patel HD (2014) Review of synthesis of 1,3,4-oxadiazole derivatives. Synth Commun 44:1859–1875. https://doi.org/10.1080/00397911.2013.879901
18. Xu C, Han Y, Xu S, Wang R, Yue M, Tian Y, Li X, Zhao Y (2020) Design, synthesis and biological evaluation of new Axl kinase inhibitors containing 1,3,4-oxadiazole acetamide moiety as novel linker. Eur J Med Chem 186:111867. https://doi.org/10.1016/j.ejmech.2019.111867
19. Chortani S, Edziri H, Manachou M, Al-Ghamdi YO, Almalki SG, Alqurashi YE, Jannet HB (2020) Novel 1,3,4-oxadiazole linked benzopyrimidinones conjugates: synthesis, DFT study and antimicrobial evaluation. J Mol Struct 1217:128357. https://doi.org/10.1016/j.molstruc.2020.128357
20. Hamdani SS, .Khan BA, Ahmed MN, Hameed S, Akhter K, Ayub K (2020) Synthesis, crystal structures, computational studies and alpha-amylase inhibition of three novel 1,3,4-oxadiazole derivatives. J Mol Struct 1200:127085. https://doi.org/10.1016/j.molstruc.2019.127085
21. Kalia V, Kumar P, Kumar S, Pahuja P, Jhaa G, Lata S (2020) Synthesized oxadiazole derivatives as benign agents for controlling mild steel dissolution: experimental and theoretical approach. J Mol Liq 313:113601. https://doi.org/10.1016/j.molliq.2020.113601
22. D.Daicoviciu A, Filip RM (2011) Oxidative photodamage induced by photodynamic therapy with methoxyphenyl porphyrin derivatives in tumour bearing rats,Folia Biol. (Praha)5712 – 9. PMID:21457649
23. Zhang ZQ, Kong LY, Xiong Y, Luo Y, Li J (2014) The synthesis of Cu(II), Zn(II) and Co(II) metalloporphyrins and their improvement to the property of Li/SOCl2 battery. J Solid State Electrochem 18:3471–3477. https://doi.org/10.1007/s10008-014-2571-3
24. Mamtmin G, Kari N, Abdurahman R (2020) 5,10,15,20-tetrakis-(4-methoxyphenyl)porphyrin film /K + ion exchanged optical waveguide gas sensor. Opt Laser Technol 128:106260. https://doi.org/10.1016/j.optlastec.2020.106260
25. Chawla G, Naaz B, Siddiqui AA (2018) Exploring 1,3,4-oxadiazole scaffold for anti-inflammatory and analgesic activities: a review of literature form 2005–2016, Mini Rev. Med Chem 18:216–233. https://doi.org/10.2174/1389557517666170127121215
26. Glomb T, Szymankiewicz K (2018) P.Swiatek,Anticancer activity of derivatives of 1,3,4-oxadiazole. Molecules 23:3361. https://doi.org/10.3390/molecules23123361
27. Verma G, Khan MF, Akthar W, Alsm MM, Akhter M, Shaquiquzzaman M (2019) A review exploring therapeutic worth of 1,3,4-oxadiazole tailored compounds. Mini Rev Med Chem 19:477–509.

https://doi.org/10.2174/1389557518666181015152433

28. Zhu JSunH, Yang Z-M, Zhu H-L (2013) Synthesis, molecular modeling and biological evaluationof 2-aminomethyl-5-(quinolin-2-yl)-1,3,4-oxadiazole-2(3H)-thione quinolone derivatives as novel anticancer agent. Eur J Med Chem 60:23–28. https://doi.org/10.1016/j.ejmech.2012.11.039
29. Zhang F, Wang X-L, Shi J, Wang S-F, Yin Y, Yang Y-S, Zhang W-M, Zhu H-L (2014) Synthesis, molecular modeling and biological evaluation of N-benzylidene-2-((5-(pyridine-4-yl)-1,3,4-oxadiazol-2-yl)thio)acetohydrazide derivatives as potential anticancer agents. Bioorg Med Chem 22:468–477. https://doi.org/10.1016/j.bmc.2013.11.004
30. Pillegowda M, Periyasamy G (2016) DFT studies on the influence of ligation on optical and redox properties of bimetallic [Au4M2] clusters. RSC Adv 6:86051–86060. https://doi.org/10.1039/C6RA14886G
31. Tlahuice-Flores A (2016) Ligand effects on the optical and chiroptical properties of the thiolated Au18 cluster. Phys Chem Chem Phys 18:27738–27744. https://doi.org/10.1039/C6CP04298H
32. Fleischmann M, Hendra PJ, Mcquillan AJ (1974) Raman spectra of pyridine adsorbed at silver electrode. Chem Phys Lett 26:163–166. https://doi.org/10.1016/0009-2614(74)85388-1
33. U.Wenning B, Pettinger HWetzel (1980) Anguler-resolved raman spectroscopy of pyridine on copper and gold electrodes. Chem Phys Lett 70:49–54. https://doi.org/10.1016/0009-2614(80)80058-3
34. Creighton JA, Alvarez MS, Weitz DA, Garoff S, Kim MW (1983) Surface-enhanced Raman scattering by molecules adsorbed on aqueous copper colloids. J Phys Chem 87:4793. https://doi.org/10.1021/j150642a007
35. G.Mengoli MM (1987) Enhanced Raman scattering from iron electrodes. Electrochim Acta 32:1239–1245. https://doi.org/10.1016/0013-4686(87)80042-7
36. Huang QJ, Li XQ, Yao JL, Ren B, Cai WB, Gao JS, Mao BW (1999) .Tian, Extending surface Raman spectroscopic studies to transition metals for practical applications: III. Effects of surface roughening procedure on surface-enhanced Raman spectroscopy from nickel and platinumelectrodes. Surf Sci 427–428. 162–166. https://doi.org/10.1016/S0039-6028(90)00258-7
37. B.H.Loo, Surface enhanced Raman scattering from pyridine adsorbed on cadmium,J. Chem. Phys.755955.https://doi.org/10.1063/1.442050
38. Lopez-Rios T, Pettenkofer C, Pockrand I (1982) Enhanced Raman scattering from aluminium films. Surf Sci 121. https://doi.org/10.1016/0039-6028(82)90231-X. L541-L544.
39. Jennings C, Aroca R, Hor AM, Loutfy RO (1984) Surface-enhanced Raman scattering from copper and zinc phthalocyanine complexes by silver and indium island films. Anal Chem 56:2033–2035. https://doi.org/10.1021/ac00276a012
40. Lund PA, Tevault DE (1984) Surface enhanced Raman spectroscopy of benzene adsorbed on vapor deposited sodium, chemical contribution to the enhancement mechanism. J Phys Chem 88:1731–1735. https://doi.org/10.1021/j150653a014
41. C.Zuo PWJagodzinski (2005) Surface-enhanced Raman scattering of pyridine using different metals: differences and explanation based on the selective formation of α-pyridyl on metal surfaces. J Phys Chem B 109:1788–1793. https://doi.org/10.1021/jp0406363
42. Muneer S, Sarfo DK, Ayoko GA, Islam N, Izake EL (2020) Gold-deposited nickel foam as recyclable plasmonic sensor for therapeutic drug monitoring in blood by surface-enhanced Raman spectroscopy. Nanomaterials 10:1756. https://doi.org/10.3390/nano10091756
43. Al-Omary FAM, Mary YS, Panicker CY, El-Emam AA, Al-Swaidan IA, Al-Saadi AA (2015) Spectroscopic investigations, NBO, HOMO-LUMO, NLO analysis and molecular docking of 5-(adamantan-1-yl)-3-anilinomethyl-2,3-dihydro-1,3,4-oxadiazole-2-thione, a potential bioactive agent. J Mol Struct 1096:1–14. https://doi.org/10.1016/j.molstruc.2015.03.049

44. Haress NG, Al-Omary F, El-Emam AA, Mary YS, Panicker CY, Al-Saadi AA, War JA, Van Alsenoy C (2015) Spectroscopic investigation (FT-IR and FT-Raman), vibrational assignments, HOMO-LUMO analysis and molecular docking study of 2-(Adamantan-1yl)-5-(4-nitrophenyl)-1,3,4-oxadiazole, Spectrochim. Acta 135:973–983. https://doi.org/10.1016/j.saa.2014.07.077
45. El-Azab AS, Mary YS, Abdel-Aziz AAM, Miniyar PB, Armakovic S (2018) Armakovic, Synthesis, spectroscopic analyses (FTIR and NMR), vibrational study, chemical reactivity and molecular docking study and anti-tubercular activity of condensed oxadiazole and pyrazine derivatives. J Mol Struct 1156:657–674. https://doi.org/10.1016/j.molstruc.2017.12.018
46. AS.Al-Tamimi YS, Miniyar LH, Al-Wahaibi AA, Armakovic (2018) Synthesis, spectroscopic analyses, chemical reactivity and molecular docking study and antitubercular activity of pyrazine and condensed oxadiazole derivatives. J Mol Struct 1164:459–469. https://doi.org/10.1016/j.molstruc.2018.03.085
47. Mary YS, Miniyar PB, Mary YS, Resmi KS, Panicker CY, Armaković S, Armaković SJ, Thomas R (2018) B.Sureshkumar,Synthesis and spectroscopic study of three new oxadiazole derivatives with detailed computational evaluation of their reactivity and pharmaceutical potential. J Mol Struct 1173:469–480. https://doi.org/10.1016/j.molstruc.2018.07.026
48. Panicker CY, Varghese HT, Ambujakhan KR, Mathew S, Ganguli S, Nanda AK, VanAlsenoy C (2010) .Mary,Ab initio and density functional theory studies on vibrational spectra of 3-{[(4-methoxyphenyl)methylene]amino}-2-phenylquinazolin-4(3H)-one. Eur J Chem 1:37–43. https://doi.org/10.5155/eurjchem.1.1.37-43
49. Mary YS, Panicker CY, Narayana B, Samshuddin S, Sarojini BK, molecular structure CVanAlsenoyFT-IR (2014) NBO analysis and first order hyperpolarizability of Methyl 4,4"-difluoro-5'-methoxy-1,1':3',1"-terphenyl-4'-carboxylate. spectrochim Acta 133:480–488. https://doi.org/10.1016/j.saa.2014.06.031
50. Renjith R, Mary YS, Panicker CY, Varghese HT, Pakozinska-Parys M, VanAlsenoy C, Al-Saadi AA (2014) Spectroscopic (FT-IR, FT-Raman) investigations and quantum chemical calculations of 1,7,8,9-tetracholoro-10,10-dimethoxy-4-{3-[4-(3-methoxyphenyl)piperazin-1-yl]propyl}-4-azatricyclo[5.2.1.0.2,6]dec-8-ene-3,5-dione, Spectrochim. Acta 129 438–450. https://doi.org/10.1016/j.saa.2014.03.077
51. Mary YS, Panicker CY, Anto PL, Sapnakumari M, Narayana B, Sarojini BK (2015) HOMO and LUMO, MEP and first order hyperpolarizability of (2*E*)-1-(2,4-Dichlorophenyl)-3-(3,4,5-trimethoxyphenyl)prop-2-en-1-one by HF and density functional methods. Spectrochim Acta 135:81–92. https://doi.org/10.1016/j.saa.2014.06.140
52. Renjith R, .Mary YS, Varghese HT, Panicker CY, Thiemann T, Shereef A, Al-Saadi AA (2015) Spectroscopic investigation (FT-IR and FT-Raman), vibrational assignments, HOMO-LUMO analysis and molecular docking study of 1-hydroxy-4,5,8-tris(4-methoxyphenyl) anthraquinone. J Phys Chem Solids 87:110–121. https://doi.org/10.1016/j.jpcs.2015.07.024
53. Echavarren AM (2016) Coinage metals in organic synthesis. Chem Soc Rev 45:4445–4447. https://doi.org/10.1039/C6CS90072K
54. L.Huang M, Arndt K (2015) .Gooben, Late transition metal-catalyzed hydroamination and hydroamidation. Chem Rev 115:2596–2697. https://doi.org/10.1021/cr300389u
55. Wang W, Cui L, L.Shi PSun (2018) C.Yue,F.Li, Reusable N-heterocyclic carbene complex catalysts and beyond: a perspective on recycling strategies. Chem Rev 118:9843–9929. https://doi.org/10.1021/acs.chemrev.8b00057
56. Budagumpi S, .Haque RA, Endud S, Rehman GU (2013) Biologically relevant silver(I)-N-heterocyclic carbene complexes: synthesis, structure, intramolecular interactions and applications. Eur J Inorg Chem 25:4367–4388. https://doi.org/10.1002/ejic.201300483
57. Kleinhans G, W.Chan AK, Leung M-Y, Liles DC, Fernandes MA, Yam VW-W, Fernandez I (2020) .Bezuidenhout, Synthesis and photophysical properties of T-shaped coinage metal complexes. Chem Eur J 26:6993–6998. https://doi.org/10.1002/chem.202000726

58. Hamze R, .Kapper SShiSC, Sylvinson D, Ravinson M, Estergreen L, .Jung MC, Tadle AC, Haiges R, Djurovich PI, Peltier JL, Jazzar R, Bertrand G, Bradforth SE, Thompson ME (2019) “Quick-silver” from a systematic study of highly luminescent, two-coordinate, d^{10} coinage metal complexes. J Am Chem Soc 141:8616–8626. https://doi.org/10.1021/jacs.9b03657
59. Diaz-Requejo MM (2008) Coinage metal catalyzed C-H bond functionalization of hydrocarbons. Chem Rev 108:3379–3394. https://doi.org/10.1021/cr078364y
60. I.Ott, On the medicinal chemistry of gold complexes as anticancer drugs,Coord. Chem. Rev.2531670–1681. https://doi.org/10.1016/j.ccr.2009.02.019
61. Mohamed AA (2010) Advances in the coordination chemistry of nitrogen ligand complexes of coinage metals. Coord Chem Rev 254:1918–1947. https://doi.org/10.1016/j.ccr.2010.02.003
62. Lopez-de-Luzuriaga JM, Monge M (2017) Luminescent aryl-group eleven metal complexes. Dalton Trans 46:2046–2067. https://doi.org/10.1039/C6DT04386K
63. Gaussian 16, Revision A, Frisch MJ, Trucks GW, Schlegel HB, Scuseria GE, Robb MA, Cheeseman JR, Scalmani G, Barone V, Petersson GA, Nakatsuji H, Li X, Caricato M, Marenich AV, Bloino J, Janesko BG, Gomperts R, Mennucci B, Hratchian HP, Ortiz JV, Izmaylov AF, Sonnenberg JL, Williams-Young D, Ding F, Lipparini F, Egidi F, Goings J, Peng B, Petrone A, Henderson T, Ranasinghe D, Zakrzewski VG, Gao J, Rega N, Zheng G, Liang W, Hada M, Ehara M, Toyota K, Fukuda R, Hasegawa J, Ishida M, Nakajima T, Honda Y, Kitao O, Nakai H, Vreven T, Throssell K, Montgomery JA Jr, Peralta JE, Ogliaro F, Bearpark MJ, Heyd JJ, Brothers EN, Kudin KN, Staroverov VN, Keith TA, Kobayashi R, Normand J, Raghavachari K, Rendell AP, Burant JC, Iyengar SS, Tomasi J, Cossi M, Millam JM, Klene M, Adamo C, Cammi R, Ochterski JW, Martin RL K. Morokuma, O. Farkas, J.B. Foresman, and D. J. Fox, Gaussian, Inc., Wallingford CT, 2016.
64. GaussView, Keith TA, Millam JM (2016)Semichem Inc., Shawnee Mission, KS,
65. Al-Otaibi JS, Mary YS, .Mary YS (2021) Adsorption of adipic acid in Al/B-N/P nanocages: DFT investigations. J Mol Model 27:113. https://doi.org/10.1007/s00894-021-04742-z
66. Al-Otaibi JS, Mary YS, .Mary YS, Kaya S, Serdaroglu G (2021) DFT computational study of trihalogenated aniline derivative’s adsorption onto graphene/fullerene/fullerene-like nanocages, X12Y12 (X = Al,B and Y = N,P). J Biomol Struct Dyn. https://doi.org/10.1080.07391102.2021.1914172
67. Lu T (2012) Multiwfn: a multifunctional wavefunction analyzer. J Comput Chem 33:580–592. https://doi.org/10.10002/jcc.22885
68. Govindachar DM, Periyasamay G (2020) DFT studies on ureido-peptide functionalized Au4M2 bimettalic nanoclusters. Chem Phys Lett 753:137612. https://doi.org/10.1016/j.cplett.2020.137612
69. Al-Otaibi JS, Mary YS, Mary YS (2022) Evidence of cluster formation of croconic acid with Ag, Au and Cu cages, enhancement of electronic properties and Raman activity. Spectrochim Acta 264:120233. https://doi.org/10.1016/j.saa.2021.120233
70. Al-Otaibi JS, Mary YS, .Mary YS, Trivedi R (2021) Theoretical investigation on the adsorption of melamine in Al12/B12-N12/P12 fullerene-like nanocages: a platform for ultrasensitive detection of melamine. Chem Pap. https://doi.org/10.1007/s11696-021-01849-8
71. Rad AS (2015) First principles study of Al-doped graphene as nanostructure adsorbent for NO2 and N2O: DFT calculations. Appl Surf Sci 357:1217–1224. https://doi.org/10.1016/j.apsusc.2015.09.168
72. Zou M, Zhang J, Chen J, Li X (2012) Simulating adsorption of organic pollutants on finite (8,0) single walled carbon nanotubes in water. Environ Sci Technol 46:8887–8894. https://doi.org/10.1021/es301370f
73. Fallahi P, Jouypazadeh H (2018) Theoretical studies on the potentials of some nanocages (Al12N12, Al12P12, B12N12, Be12O12, C12Si12, Mg12O12 and C24) on the detection and adsorption of tabun molecule: DFT and TD-DFT study. J Mol Liq 260:138–148. https://doi.org/10.1016/j.molliq.2018.03.085

74. J.Jiang TYan, Cui D, Wang J, Salehabadi M, Shen J (2020) Quantum chemical study on the potential application of pristine and BN-doped graphynes for carac drug detection. Appl Surf Sci 146758. https://doi.org/10.1016/j.apsusc.2020.146758
75. Rad AS (2015) Adsorption of acetyl halide molecules on the surface pristine and Al-doped graphene: Ab initio study. Appl Surf Sci 355:233–241. https://doi.org/10.1016/j.apsusc.2015.07.113
76. Glendening ED, Reed AE, Carpenter JE, Weinhold F (2003) NBO version 3.1. Gaussian Inc., Pittsburg, PA
77. Costa RA, .Barros GA, da Silva JN, Oliveira KM, Bezerra DP, Soares MBP (2021) .Costa, Experimental and theoretical study on spectral features, reactivity, solvation, topoisomerase I inhibition and in vitro cytotoxicity in human HepG2 cells of guadiscine and guadiscidine aporphine alkaloids. J Mol Struct 1229:129844. https://doi.org/10.1016/j.molstruc.2020.129844
78. Al-Otaibi JS, Mary YS, .Mary YS, Ullah Z (2022) Adsorption behavior and solvent effects of an adamantane-triazole derivative on metal clusters-DFT simulation studies. J Mol Liq 345:118242. https://doi.org/10.1016/j.molliq.2021.118242
79. Al-Otaibi JS, Mary YS (2022) .Mary, Adsorption of a thione bioactive derivative over different silver/gold clusters – DFT investigations. Comput Theor Chem 1207:113497. https://doi.org/10.1016/j.comptc.2021.113497
80. Alharthi FA, Al-Zaqri N, Alsalme A, Al-Taleb A, Pooventhiran T, Thomas R (2021) Excited-state electronic properties, structural studies, noncovalent interactions and inhibition of the novel severe acute respiratory syndrome corona virus 2 proteins in ripretinib by first principle simulations. J Mol Liq 324:115134
81. Surendar P, Pooventhiran T, Al-Zaqri N, Rajam S, Rao DJ (2021) Synthesis of three quasi liquid Schiff bases between hexanal and adenine, cytosine and l-leucine, structural interpretation, quantum mechanical studies and biological activity prediction. J Mol Liq 117305. https://doi.org/10.1016/j.molliq.2021.117305
82. Alsalme A, Pooventhiran T, Al-Zaqri N, Rao DJ (2021) Structural, physic-chemical landscapes, ground state and excited state properties in different solvent atmosphere of avapritinib and its ultrasensitive detection using SERS/GERS on self assembly formation with graphene quantum dots. J Mol Liq 322:114555
83. Al-Zaqri N, Pooventhiran T, Rao DJ, Alsalme A, Warad I (2021) Structure, conformational dynamics, quantum mechanical studies and potential biological activity analysis of multiple sclerosis medicine ozanimod. J Mol Struct 1227:129685. https://doi.org/10.1016/j.molstruc.2020.129685
84. Al-Zaqri N, Pooventhiran T, Alsalme A, I.Warad AM (2020) Structural and physic-chemical evaluation of melatonin and its solution state excited properties with emphasis on its binding with novel corona virus proteins. J Mol Liq 318:114082. https://doi.org/10.106/j.molliq.2020.114082
85. BhattacharyyaTPooventhiranU, Rao DJ, Chandramohan V, Karunakar P, Irfan A, Mary YS (2020) Detailed spectra, electronic properties, qualitative non-covalent interaction analysis, solvatochromism, docking and molecular dynamics simulations in different solvent atomosphere of cenobamate. Struct Chem. https://doi.org/10.1007/s11224-020-01607-8
86. E.Runge EKU (1984) .Gross, Density-functional theory for time-dependent systems. Phys Rev Lett 52:997. https://doi.org/10.1103/PhysRevLett.52.997
87. A.Bhunia S, Manna S, Mistri A (2015) Synthesis, characterization, TDDFT calculation and biological activity of tetradentate ligand based square pyramidal Cu(II) complexes, RSC Adv. 567727–67737.https://doi.org/10.1039/C5RA12324K
88. K.Stevenson AF (2016) General calibration of microbial growth in microplate readers. Sci Rep 6:38828. https://doi.org/10.1038/srep38828
89. Chen B, Liu M, Zhang L, Huang J, Yao J, Zhang Z (2011) Polyethylenimine-functionalized graphene oxide as an efficient gene delivery vector. J Mater Chem 21:7736–7741. https://doi.org/10.1039/C1JM10341E

90. Y.Pan H, Wu L, Li (2011) Water soluble poly (N-isopropylacrylamide) graphene sheets synthesized via click chemistry for drug delivery. Adv Func Mater 21:2754–2763. https://doi.org/10.1002/adfm.201100078
91. E.vanStevendaal MHM, vanHest JCM (2021) A.F.Mason, Functional interactions between bottom-up synthetic cells and living matter for biomedical applications, ChemSystemsChem. 3e2100009. https://doi.org/10.1002/syst.202100009

Figures

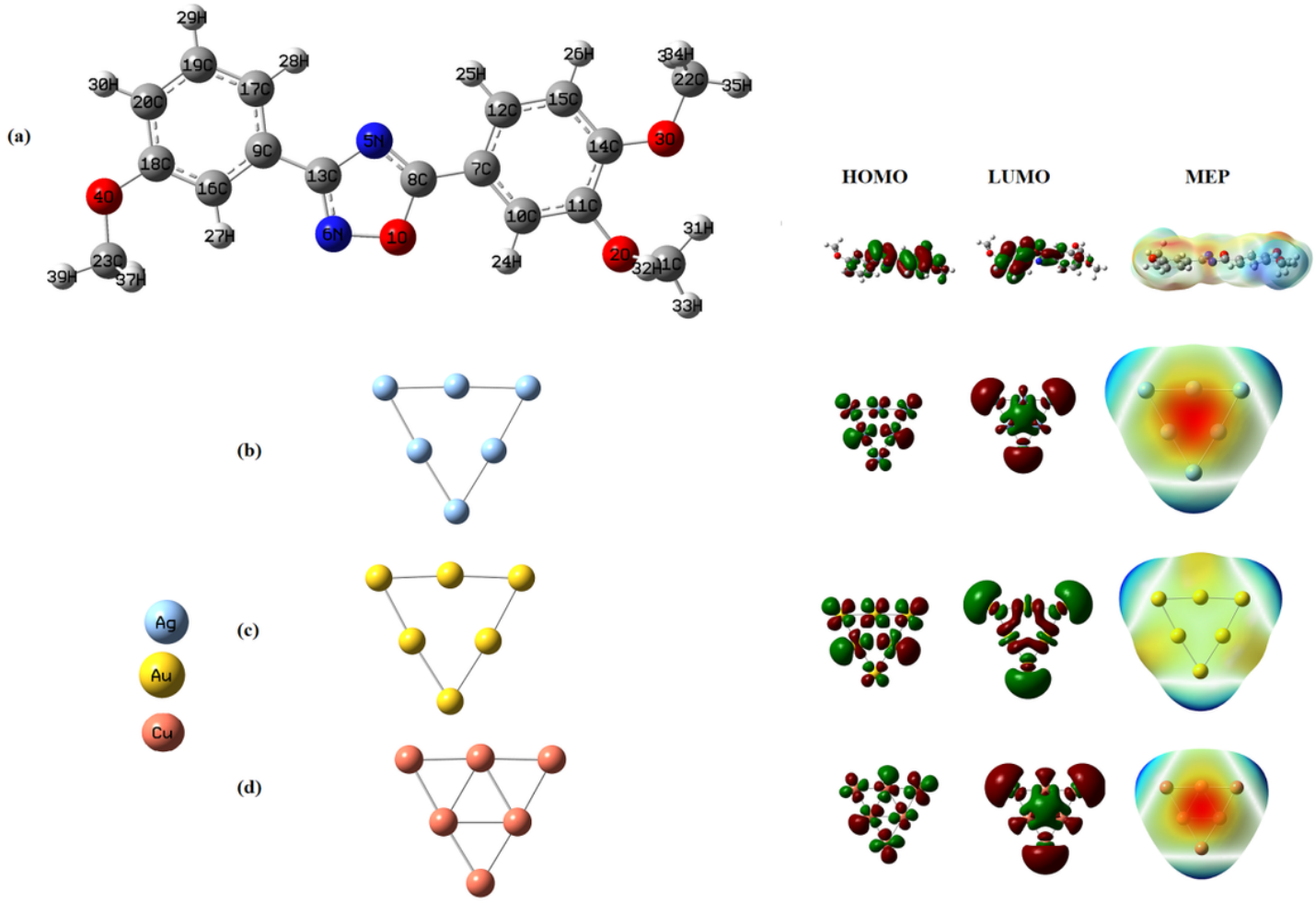

Figure 1

Optimized geometries, FMOs and MEP plot of (a) DPMO (b) Ag_6 (c) Au_6 (d) Cu_6

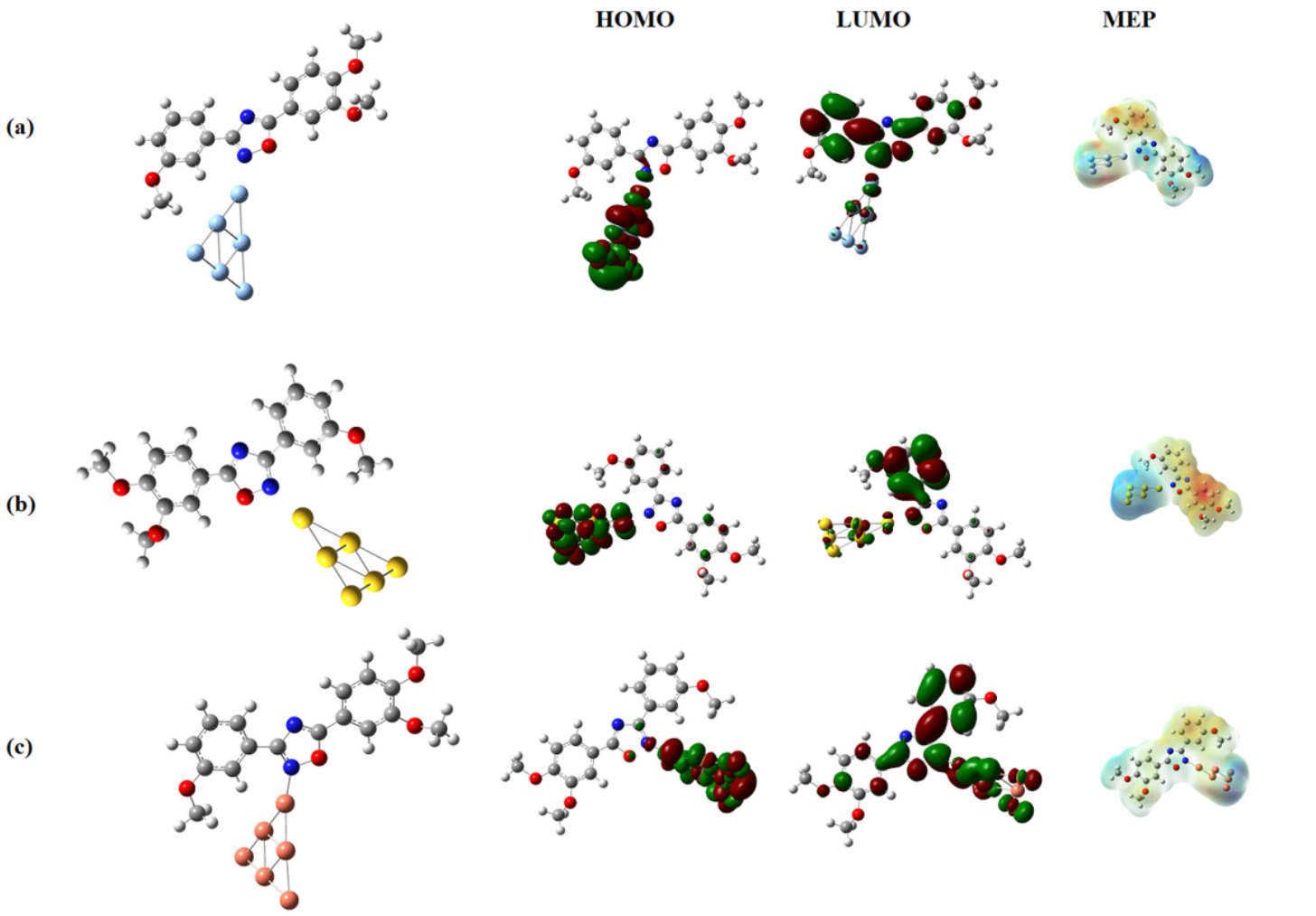

Figure 2

Optimized geometries, FMOs and MEP plot of (a) DPMO-Ag_6 (b) DPMO-Au_6 (c) DPMO-Cu_6

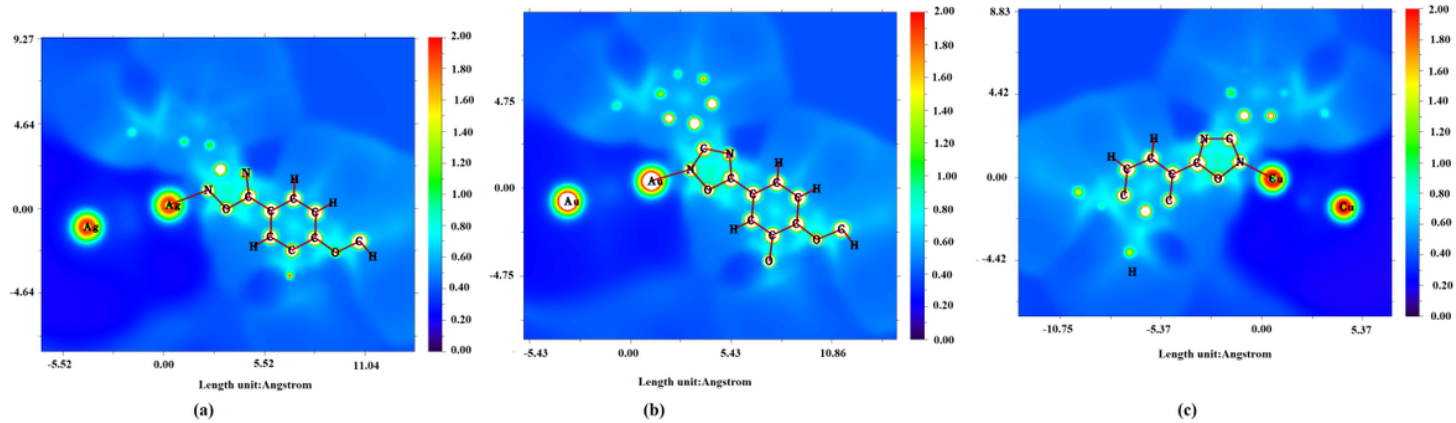

Figure 3

ALIE plots of (a) DPMO-Ag_6 (b) DPMO-Au_6 (c) DPMO-Cu_6

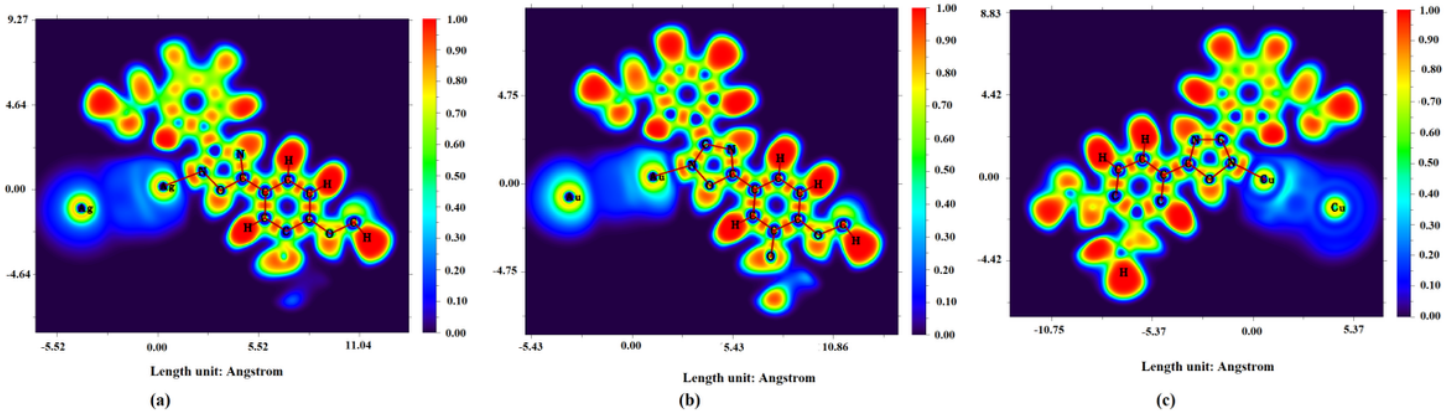

Figure 4

ELF plots of (a) DPMO-Ag_6 (b) DPMO-Au_6 (c) DPMO-Cu_6

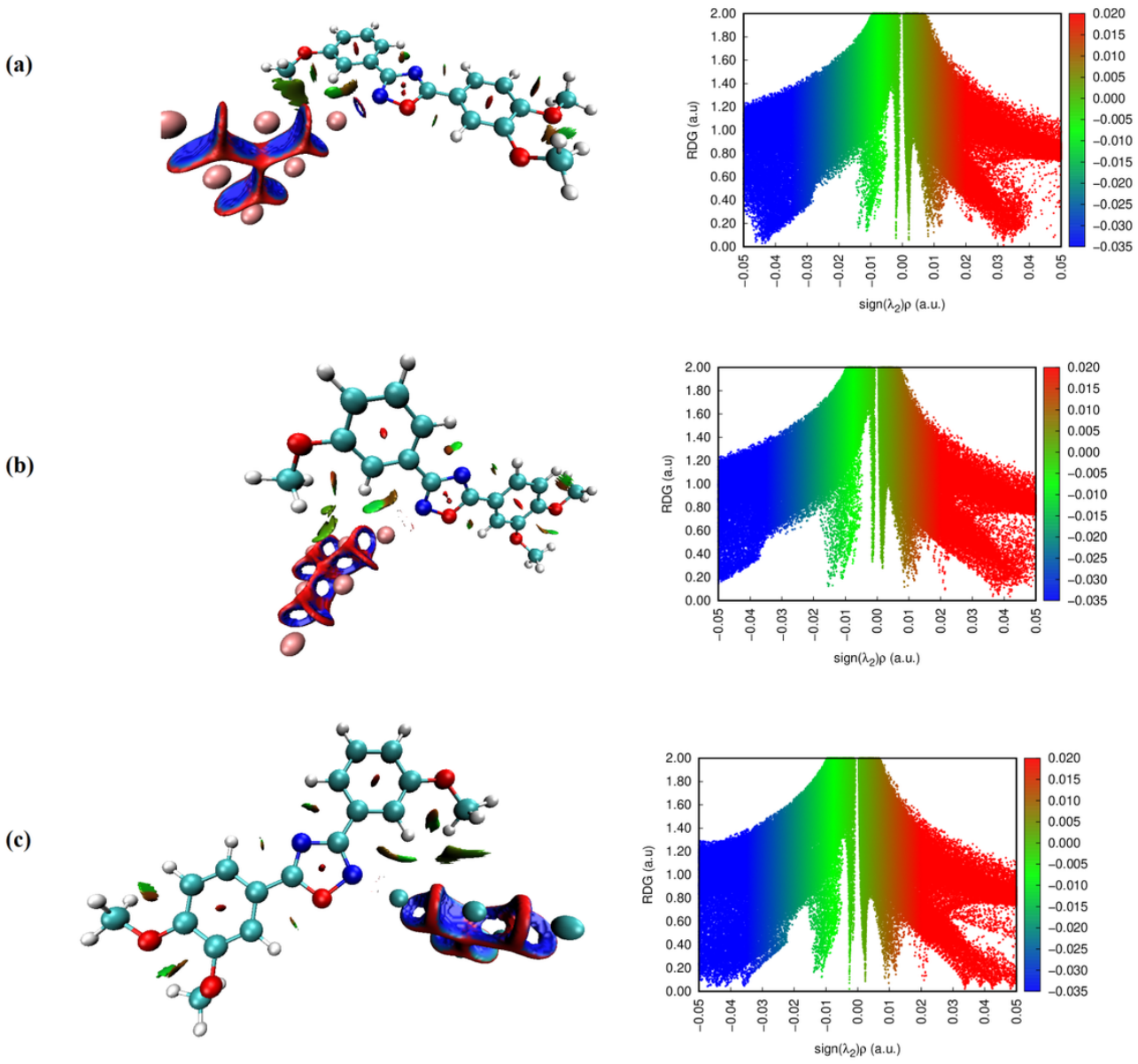

Figure 5

NCI plots of (a) DPMO-Ag_6 (b) DPMO-Au_6 (c) DPMO-Cu_6

Supplementary Files

This is a list of supplementary files associated with this preprint. Click to download.

- graphicalabstract.docx
- supplementary.doc